

ARTICLES

Incorporation of Vanadium in Mesoporous MCM-41 and Microporous AFI Zeolites

K. J. Chao,* C. N. Wu, and H. Chang

Department of Chemistry, National Tsinghua University, Hsinchu, Taiwan 300, R.O.C.

L. J. Lee

Precision Instrument Development Center, NSC, Taiwan, R.O.C.

Shu-fen Hu

Material Science Center, National Tsinghua University, Hsinchu, Taiwan 30043, R.O.C.

Received: February 18, 1997; In Final Form: May 28, 1997[®]

Vanadium-containing silicate MCM-41 (V-MCM-41) zeolite and aluminophosphate AFI (VAPO-5) zeolite were synthesized and characterized by spectroscopic techniques. In as-synthesized form, the vanadyl ions ($V^{IV}=O$)²⁺ were found to be the major vanadium species in the form of atomic dispersion on AFI by EPR and to exist simultaneously with tetrahedral (T_d) V^{5+} in MCM-41 by UV-vis. ²⁹Si MAS NMR investigations suggested that the vanadium ions might attach to MCM-41 through interaction with the silanol groups on the internal wall of hexagonal tubes. The V^{5+} (in T_d) ions are incorporated into the lattice of MCM-41 during synthesis, while the VO^{2+} (in T_d) is the loosely bound V species. The results of Raman spectroscopy indicated that the rodlike aggregation of cationic surfactant (cetyltrimethylammonium bromide, CTAB) was encapsulated in the intrachannel space of synthetic MCM-41 as in an aqueous solution. After calcination and hydration, the V^{4+} species in as-synthesized V-MCM-41 was totally oxidized to +5 as shown by UV-vis and EPR spectroscopies, and they further aggregated as two-dimensional vanadate chain species that were nonuniformly deposited on the wall of MCM-41 channels as verified by Raman and HREM with EDS spectroscopies, while the V^{5+} species of synthetic V-MCM-41 remains stable in a tetrahedral coordination. Comparatively, two types of VO^{2+} ions were observed in as-synthesized VAPO-5 by EPR and they could be oxidized by calcination treatment. The presence of water vapor facilitates the oxidation of ($V^{IV}=O$)²⁺ and the formation of V_2O_5 cluster instead of isolated ($V^{IV}=O$)³⁺ species.

Introduction

Vanadium oxide loaded metal oxides^{1–4} and vanadium-incorporated molecular sieves^{5–17} have been considered as selective oxidation catalysts. The activity and selectivity of these catalysts were found to be sensitive to the nature of V species in the matrix, which includes oxidation state, coordination condition, dispersion, and stability.^{1–4,8–11} Besides dispersing and stabilizing vanadium oxides, structural features of microporous and macroporous supports also have effect on the form of vanadium species and its catalytic behavior. Vanadium species were doped on SiO_2 , TiO_2 , and Al_2O_3 supports via ion-exchange and wet-impregnation methods^{3,4} and were found to be in the +5 state and existed in three forms: monomeric vanadyls, the one- or two-dimensional vanadate chains, and the crystallites of V_2O_5 . In the case of synthetic V-MFI and V-MEL zeolites, by substituting framework Si or bonding to defect centers of the zeolitic framework, both V^{5+} and V^{4+} were observed to exist simultaneously in either tetrahedral or square pyramidal coordinations.^{9b,12} For synthetic VAPO, vanadium was incorporated in acid medium instead of under basic condition in synthesizing aluminosilicate and silicate molecular sieves and was observed to mainly exist in well-dispersed

monomeric vanadyl ($V^{IV}=O$) form,^{13–17} whether it was generated by substituting framework Al or P is a matter of debate.^{13–15} Rigutto and van Bekkum suggested the replacement of P^{5+} by V^{4+} ;¹⁵ Montes *et al.* proposed the existence of neutrality between VO^{2+} ion and two $-Al-OH$ groups;¹³ Weckhuysen *et al.*¹⁶ and Lohse *et al.*¹⁷ observed no spectroscopic evidence for true isomorphous substitution of V^{4+} into the tetrahedral lattice of $AlPO_4$ molecular sieves.

Very recently the family of novel mesoporous silicates, M41S,^{18,19} were reported to be the potential matrix for vanadium species to fillup the gap between microporous and macroporous supports and to enlarge the utilization of zeolites in oxidation reactions for bulky compound.^{5–7} Vanadium ions could be introduced to mesoporous zeolites either by direct hydrothermal synthesis^{5,6} or by impregnation method.⁷ Gontier *et al.* observed that vanadium cations in synthetic V-MCM-41 were probably in a coordination state as that in aqueous solution without direct chemical bonding to the silicate framework.⁶ Morey *et al.* prepared the mesoporous V-MCM-48 material using an impregnation method and, through UV-vis measurement, they suggested that hydroxyl groups on the wall of MCM-48 material were employed as anchoring sites for vanadium ions to form pseudotetrahedral $O_{3/2}V=O$ graft on the mesoporous wall.⁷

The framework of mesoporous M41S differs from that of microporous zeolite of three-dimensional tetrahedral network

* To whom correspondence should be addressed.

® Abstract published in *Advance ACS Abstracts*, July 1, 1997.

and is constructed from amorphous silica around the rodlike micellar template of cationic surfactant.^{18–20} Therefore, no evidence of long-range ordering along the channel wall was observed on M41S. ²⁹Si MAS NMR shows that M41S possesses comparatively many more Si–OH groups than microporous aluminosilicate and silicate zeolites, and such hydroxyl groups are similar to defect sites on microporous zeolites and can act as anchors for the attachment of transition-metal species via intermolecular condensation.

In this study, vanadium-containing MCM-41 and AlPO₄-5 molecular sieves were synthesized. The structure and nature of vanadium species as well as their interactions with MCM-41 and AlPO₄-5 supports during redox treatments are compared using EPR, Raman, UV–vis, and ²⁹Si MAS NMR spectroscopic techniques. In addition, the distribution of vanadium on MCM-41 framework was studied by HRTEM (high-resolution transmission electron microscopy) with EDS (energy-dispersive X-ray spectroscopy). Through these methods we could distinguish the effect of interactions between vanadium species and either the surface Si–OH (in mesoporous framework), or Al–OH and P–OH (in microporous framework) and provide information about the ease of interconversion of V⁴⁺ to V⁵⁺ under oxidation and reduction treatments and shed light on the potential role of vanadium in redox reaction. In addition to the aforementioned analyses, the structure of templating surfactant micelle in mesoporous MCM-41 was also monitored by Raman spectroscopy.

Experimental Section

The V-MCM-41 was prepared by direct hydrothermal synthesis.²¹ An aqueous solution of vanadyl sulfate (VOSO₄·5H₂O, Fluka) was added slowly into an aqueous sodium silicate solution containing CTAB (cetyltrimethylammonium bromide, TCI). The molar ratios of reactant mixtures were 1.0 SiO₂:*x* VO₂:*y* CTAB:*z* H₂O, *y* = 0.58, *z* = 86, and *x* = 0.033, 0.02, 0.01, and 0.00 to give MCM-41 samples denoted as SiV30, SiV50, SiV100, and Si-MCM-41, and *x* = 0, *y* = 0.12, and *z* = 241 for Si–F.²¹ After stirring for 30 min, a dilute sulfuric acid solution was then added into the above hydrogel to adjust the pH value to 11–12, and the resulting mixture was stirred for an additional hour and heated at 100 °C for 6 d in a PTFE-lined autoclave. The final products were recovered by filtration, followed by washing with deionized water or ethanol, drying at 70 °C, and calcining at 540 °C (for 1 h under N₂ and 10 h under air). The bulk Si/V atomic ratios of V-MCM-41 materials were ~52 (SiV30), ~105 (SiV50), and ~385 (SiV100), as measured by ICP-AES. N₂ adsorption isotherms of these V-MCM-41 materials showed a typical type IV isotherm of cylindrical mesopores with 3.0 nm in diameter.²¹

The reactants of VAPO-5 synthesis were 85% H₃PO₄ (Merck), pseudoboehmite (Capatal B, 70% Al₂O₃ and 30% H₂O), vanadyl sulfate (VOSO₄·E5H₂O, Fluka), and tripropylamine (Merck). The reactant gel was prepared according to the following steps: 15.4 g of pseudoboehmite was added slowly to a 3.4 M orthophosphoric acid under intense stirring over a period of 2 h, the resulting mixture was stirred for another 2 h, and subsequently, a 1.1 M VOSO₄ solution and 10 mL of tripropylamine were added dropwise. The final reactant mixture, with a molar ratio of 0.95 P₂O₅:1 Al₂O₃:0.1 VO:1 Pr₃N:40 H₂O, was stirred for 2 h, and then was charged in a teflon-lined stainless-steel autoclave and kept in a preheated oven at 150 °C for 2 days. After crystallization, the greenish crystals were washed with deionized water and dried at 70 °C. The organic template molecules encapsulated in VAPO-5 were removed upon

calcination under a flow of dry O₂ or air at 500 °C for 36 h. A part of the calcined sample was also reduced by H₂ at 500 °C for 8 h.

EPR spectra were recorded at 77 and 293 K with a Bruker ER200D-SRC spectrometer operated in a X-band. The microwave power was 2.0 mW with a resonance frequency of *ca.* 9.60 GHz by using 100 kHz modulation. The *g* values of these signals were measured relative to DPPH (*g* = 2.0036). ²⁹Si MAS NMR spectra were acquired by a Bruker MSL-200 NMR instrument. Typically, more than 3000 free induction decays were accumulated with a $\pi/4$ flip angle and 10 s interval. Static ⁵¹V NMR spectra were obtained on a Bruker AMX-300 NMR spectrometer at frequency of 78.9 MHz. UV–vis diffuse reflectance spectra were measured with a Hitachi U-3500 spectrometer equipped with a reflectance attachment and BaSO₄ was used as reference substance. Raman spectra were obtained with a Spex spectrometer. The scattered photons were detected by RCA 31034A photomultiplier with an SSR model 1106 photo counter. The sample was excited by a Spectra Physics 216 argon ion laser at 5145 Å at a power of 70 mW. Typically, the scanning rate and the resolution of the spectrum were 2 cm^{–1}/s and 5 cm^{–1}, respectively. Acidity was determined by means of temperature-programmed desorption (TPD) of ammonia with on-line titration. Prior to TPD run, the sample was dehydrated by heating at 2 °C/min to 300 °C, kept at 300 °C for 2 h, and cooled down to room temperature. Ammonia was adsorbed at room temperature and the sample was subsequently purged by flowing Ar at 150 °C for 8 h to remove excess and physically adsorbed ammonia. The sample was then heated at 5 °C/min from 150 to 600 °C under flowing dry Ar (30 mL/min). The desorbed ammonia was trapped in a solution of saturated boric acid and 1 M NH₄Cl and was titrated by sulfamic acid. The number of milliequivalents of NH₃ evolved per gram of sample is calculated from the volume of titrant (with 0.20 mg of NH₃/mL) used vs temperature. Differential thermal (DTA) and thermogravimetric thermal (TG) analyses were performed using flowing Ar (100 cm³/min) through a Seiko TG/DTA 300-10 apparatus. Chemical compositions of individual microcrystallites of calcined V-MCM-41 were examined by EDS using a JEM-2010 electron microscope operating at 200 kV.

Results

EPR Spectroscopy. Figure 1 displays the typical EPR spectra of V-MCM-41 samples (SiV30) under various conditions. All of the as-synthesized V-MCM-41 samples show EPR spectra characteristic of well-dispersed vanadyl ions (V^{IV}=O)²⁺ in an axially symmetric crystal field. The spin density of signals increases almost linearly with vanadium loading. The persistence of an anisotropic hyperfine structure from 77 K to room temperature of as-synthesized SiV30 sample reveals the existence of isolated vanadium species. The axially symmetric EPR signal of vanadyl species completely disappeared upon oxidation of V-MCM-41 in air at 540 °C; this indicates that all the (V^{IV}=O)²⁺ ions have been oxidized to (V^V=O)³⁺. Subsequent reduction in H₂ at 500 °C recovers the original hyperfine structure with lower intensity than those of as-synthesized samples; this is probably due to the variation in the dispersion of reduced (V^{IV}=O)²⁺.

Figure 2 shows the EPR spectra of as-synthesized, calcined, and reduced VAPO-5 samples. The spectrum of as-synthesized form possesses two axially symmetric signals with hyperfine splitting, typical of (V^{IV}=O)²⁺ in two slightly different environment.^{13–17} After calcination under dry O₂ or air at 500 °C, the signal intensity is approximately 1 order of magnitude lower than that obtained from as-synthesized VAPO-5. This

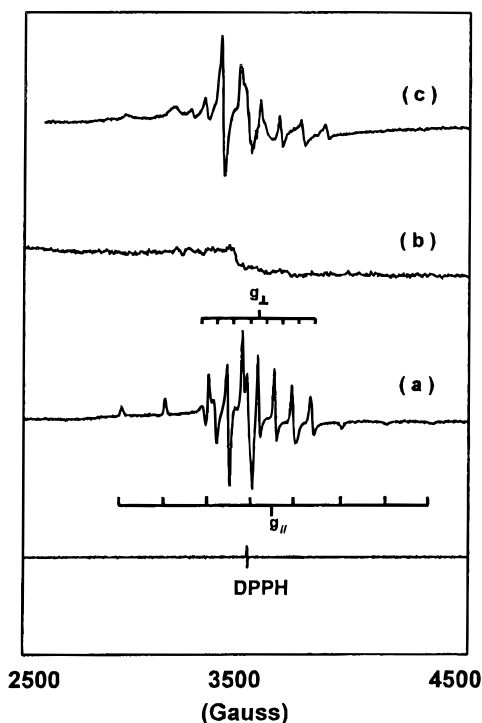


Figure 1. EPR spectra of (a) as-synthesized, (b) calcined, and (c) H_2 reduced SiV30 samples at 77 K.

indicates that some of the V^{4+} have been oxidized to V^{5+} and some still remains in the +4 state of a highly dispersed form after calcination. Upon exposure to H_2 at 500 °C, vanadium was found to be reduced and to give similar EPR spectrum as the as-synthesized VAPO-5. This reduced sample reacts quickly and efficiently with O_2 at room temperature to produce O_2 radical, as demonstrated by EPR spectra at 293 and 77 K (Figure 2d). O_2^- is very unlikely to form from $(\text{V}^{\text{IV}}=\text{O})^{2+}$ and probably is adsorbed on severely reduced vanadium species (V^{3+} , V^{2+} , etc. existed with V^{4+}), which are EPR silent at and above 77 K. These O_2 radicals are very effective in hydrocarbon oxidation, particularly, in the oxidative dehydrogenation of alkanes.^{22,23}

If VAPO-5 sample was calcined in air containing some water vapor, the intensity of EPR signal would reduce to 2 orders of magnitude lower than that of the synthetic form; this was also reported by previous investigations.^{13,16,17} The presence of water vapor will help the generation of V_2O_5 cluster from $(\text{V}^{\text{V}}=\text{O})^{3+}$ as characterized by Raman (see sections below). The calcined sample above was subsequently reduced under H_2 at 500 °C to recover its EPR signal and to produce inactive V^{4+} species that no longer could generate O_2 radical species under O_2 environment.

^{29}Si MAS NMR Spectroscopy. Figure 3 shows ^{29}Si MAS NMR spectra of synthetic Si-MCM-41 and V-MCM-41 (SiV30 and SiV100) samples with different V loadings. No extra peak associated with Si—O—V bonding was found in Figure 3. ^{29}Si NMR spectra could be deconvoluted into three Gaussian peaks with chemical shift of -110.0 (Q_4), -100.1 (Q_3), and -91.2 (Q_2) ppm corresponding to $\text{Si}(\text{OSi})_4$, $\text{Si}(\text{OSi})_3\text{OH}$ and $\text{Si}(\text{OSi})_2(\text{OH})_2$, respectively, and these NMR peaks were used to monitor the relative concentrations of the silicon species. As the concentration of vanadium increases, the relative intensities of $\text{Si}(\text{OSi})_3\text{OH}$ and $\text{Si}(\text{OSi})_2(\text{OH})_2$ signals related to silanol groups decrease while that of Q_4 signal increases by the contribution of both $\text{Si}(\text{OSi})_4$ and $\text{Si}(\text{OSi})_{4-n}(\text{OV})_n$ species ($n = 0, 1, \text{ or } 2$); the signals of $\text{Si}(\text{OSi})_{4-n}(\text{OV})_n$ could not be resolved from $\text{Si}(\text{OSi})_4$ signal.⁸ This implies that there is interaction between

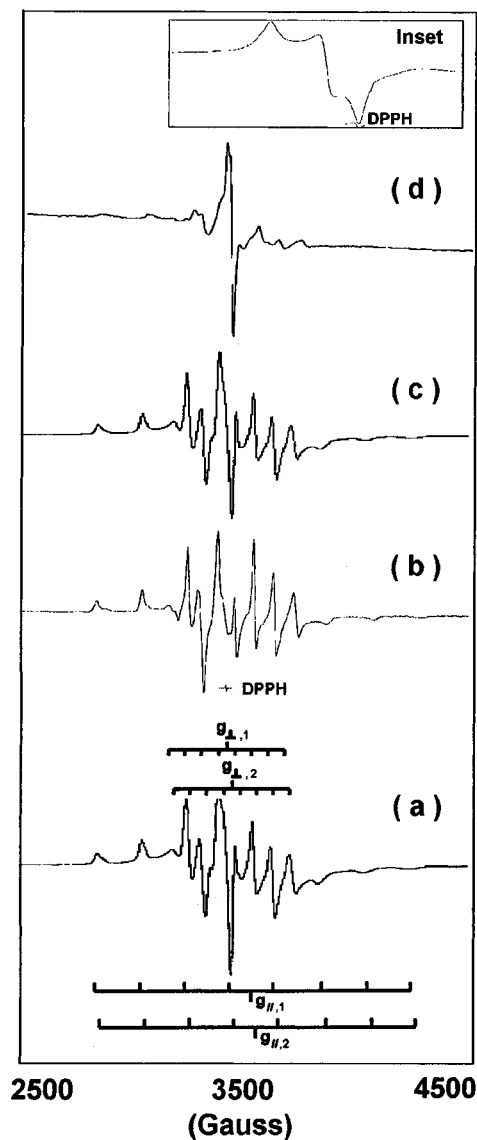


Figure 2. EPR spectra of (a) as-synthesized, (b) calcined, (c) H_2 reduced, and (d) O_2 -adsorbed (after reduction) VAPO-5 samples at 77 K (inset: O_2 radical signal of (d)).

vanadium ions and hydroxyl groups of the silica-based cylindrical walls. The interaction of vanadyl cation brought about a decrease in the number of Si—OH species and this was also observed on microporous V-ZSM-12 by ^{29}Si MAS NMR by Moudrakovski *et al.*⁸ They suggested that incorporation of vanadium into ZSM-12 zeolite took place through interaction with the silanol groups at defect sites of zeolitic framework. Thus, during synthesis the vanadyl ions (VO^{2+} or VO^{3+}) are suggested to be bound to the tubular wall of MCM-41 by condensation with silanol groups of wall.

^{51}V NMR Spectroscopy. Figure 4 shows the calcined, hydrated ^{51}V NMR spectra of V-MCM-41 (SiV30) and VAPO-5 samples. In the presence of water, vanadium(V) in a calcined SiV30 seems to exist predominantly in a distorted octahedral environment and this gives rise to a broad band centered at -293 ppm, resembling the feature of the surface vanadium oxide phase on hydrated silica.¹ Vanadium species deposited on calcined MCM-41 seem not to be monodispersed but aggregated to form hydrated amorphous V_2O_5 -like cluster on the walls of channels in the mesoporous sample.

Calcined, hydrated VAPO-5 material possesses an axially symmetric ^{51}V NMR powder pattern with anisotropic chemical shift parameters and of approximate values -326 and -876

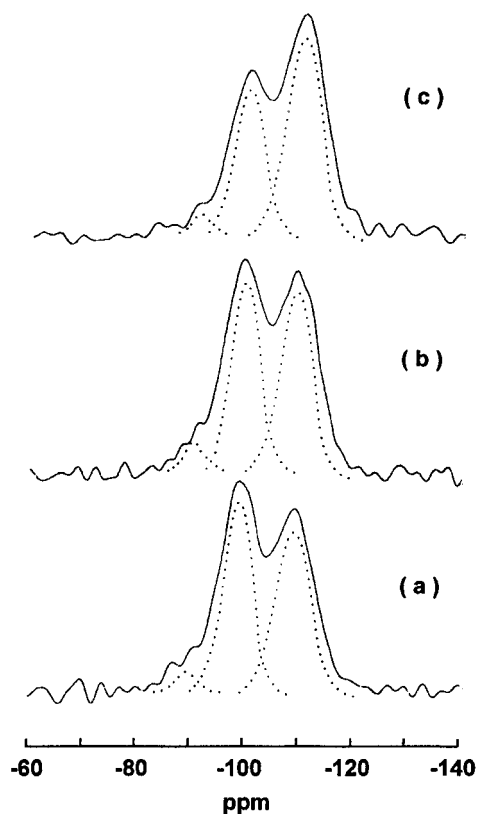


Figure 3. ^{29}Si MAS NMR spectra of as-synthesized (a) Si-MCM-41, (b) SiV100, and (c) SiV30 samples.

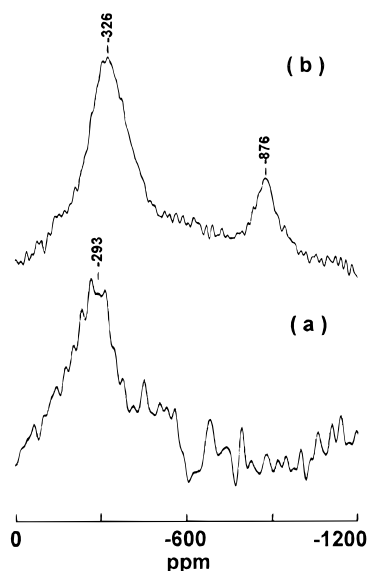


Figure 4. Static ^{51}V NMR spectra of calcined and hydrated (a) SiV30 and (b) VAPO-5 samples.

ppm, respectively, corresponding to a single square pyramidal vanadyl species; and this is in good agreement with the previous study.¹⁵

DR UV-vis Spectroscopy. The differential reflectance UV-vis spectra of hydrated, as-synthesized, and calcined V-MCM-41 and VAPO-5 are shown in Figure 5. As-synthesized V-MCM-41 (pale violet) samples exhibit two intense absorption bands at around 280 and 340 nm in the UV region, and one weak band at about 605 nm in the visible region, as shown in Figure 5a. The doublet bands of 280 and 340 nm correspond to the low-energy charge-transfer (CT) bands associated with V–O electron transfer (π) $t_2 \rightarrow$ (d)e and (π) $t_1 \rightarrow$ (d)e, respectively for tetrahedrally coordinated and colorless

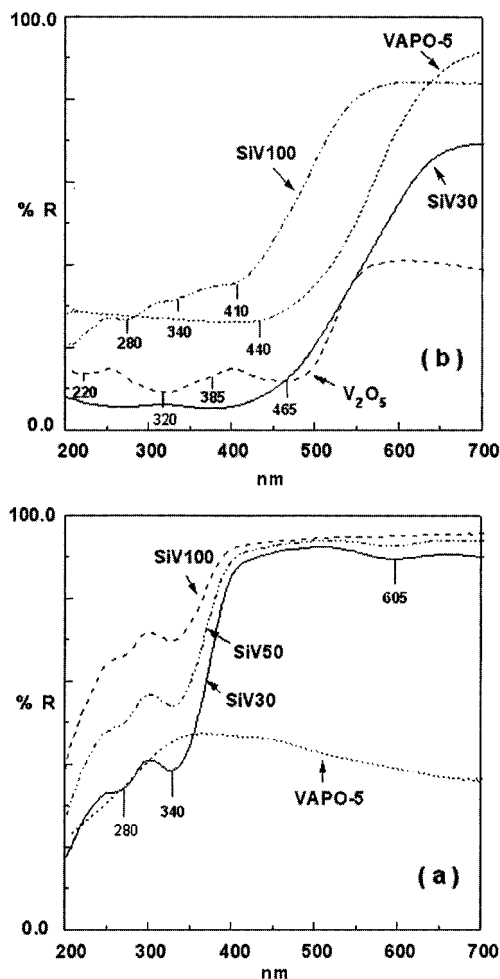


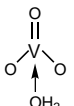
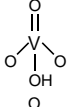
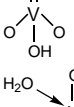
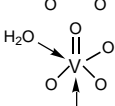
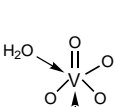
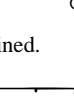

Figure 5. Diffuse-reflectance UV-vis spectra of (a) as-synthesized and (b) calcined V-MCM-41 and VAPO-5 materials at ambient condition.

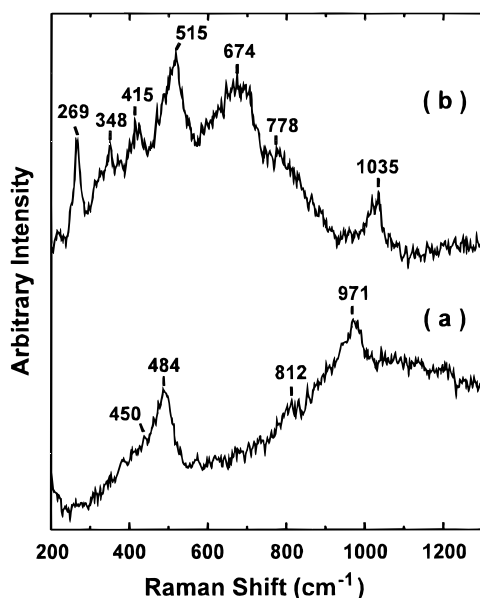
V^{5+} ions.^{9b,10,12} The band of 610 nm is assigned to the d–d transition of the VO^{2+} ions, $b_2(d_{xy}) \rightarrow a_1(d_{x^2-y^2})$, this absorption gives a sample with pale violet color,^{9b,12} while the as-synthesized form of VAPO-5 sample did not exhibit any band in the region 250–340 nm, suggesting the absence of detectable amounts of V^{5+} in T_d environments.

After calcination, the V-MCM-41 sample became white to pale yellow and after contact with air it turned into intensive yellow. The disappearance of an absorption band about 610 nm is due to the oxidation of V^{4+} to V^{5+} . In calcined and hydrated SiV100 sample (Si/V \sim 385), the doublet bands of 280 and 340 nm, associated with the tetrahedral V^{5+} ions, still remained and an additional absorption band of \sim 410 nm, corresponding to the CT transition of the $\text{V}=\text{O}$ double bond of square-pyramidal V^{5+} ions, was observed. With increasing vanadium content, the calcined and hydrated SiV30 (Si/V \sim 52) sample possesses a very broad absorption band around 320–500 nm, this probably relates to an octahedral V^{5+} species. Most of the UV-vis spectra of as-synthesized and calcined samples show the presence of V_2O_5 that typically exhibits absorption bands around 220, 320, 385, and 465 nm. The calcined, hydrated VAPO-5 sample exhibited a very broad band at 250–550 nm as that of calcined SiV30, indicating the presence of octahedral V^{5+} species. The above results are summarized in Table 1.

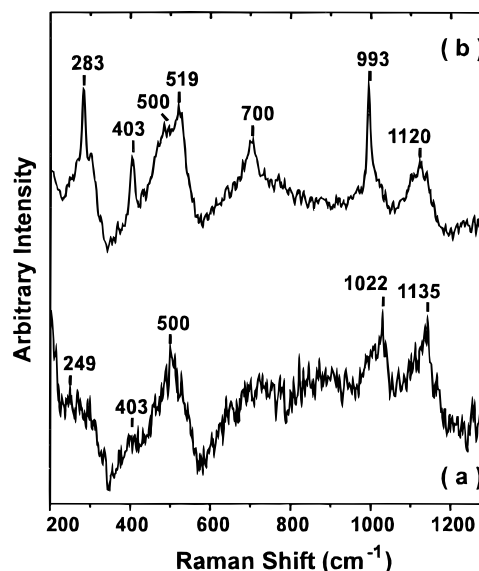
Raman Spectroscopy. Figure 6 shows the Raman spectra of calcined, hydrated Si-MCM-41 and V-MCM-41 (SiV30) samples. The pure siliceous MCM-41 framework possesses Raman bands at 450 and 812 cm^{-1} (siloxane bridges), 484 cm^{-1} (fourfold siloxane rings), and 971 cm^{-1} (surface silanol groups),

TABLE 1: Vanadium Species in V-MCM-41 and VAPO-5 Based on EPR and UV-Vis Analyses

sample ^a	UV-vis (nm)	EPR	V species	symmetry
a.s. V-MCM-41	~605	VO ²⁺		V ⁴⁺ in <i>T_d</i>
	280, 340	no		V ⁵⁺ in <i>T_d</i>
calc. V-MCM-41	280, 340	no		V ⁵⁺ in <i>T_d</i>
	410	no		V ⁵⁺ in square pyramidal
	320–500	no		V ⁵⁺ in <i>O_h</i>
a.s. VAPO-5		VO ²⁺		V ⁴⁺
calc. VAPO-5	330–500	VO ²⁺		V ⁵⁺ in <i>O_h</i> , V ⁴⁺

^a a.s. = as synthesized, calc. = calcined.**Figure 6.** Raman spectra of calcined (a) Si-MCM-41 and (b) SiV30 materials.

which express the features of amorphous-like silica structure.²⁰ The introduction of vanadium species in the MCM-41 structure gives Raman bands at 269, 348, 415, 515, 674, 778, and 1035 cm⁻¹. The Raman band of 1035 cm⁻¹ corresponds to the stretching frequency of a terminal of V=O group bonded to the silicate MCM-41 host, similar to those observed for vanadium oxytrihalides of VOF₃ (at 1053 cm⁻¹),²⁴ VOCl₃ (at 1035 cm⁻¹),²⁵ and VOB₃ (at 1028 cm⁻¹),²⁶ and a monomeric vanadyl species bonded to the SiO₂ support (at 1042 cm⁻¹).^{3a} The Raman band at 269 cm⁻¹ can be ascribed to the V–O–V bending mode; the bands centered around 415, 515, and 674 cm⁻¹ may correlate with the V–O–V stretching vibrations^{1,2} and they may show overlap with the bands belong to the amorphous silicates structures.

**Figure 7.** Raman spectra of calcined VAPO-5 samples: upon calcination (a) in dry O₂ environment and (b) in air with little humidity.

The V₂O₅ crystallites possess sharp Raman bands at 994 cm⁻¹ (symmetric stretching of V=O groups), 702, 527, and 404 cm⁻¹ (V–O–V stretching), and 284 cm⁻¹ (V–O–V bending mode).^{1–4} The Raman bands of V-MCM-41 are similar to those of crystalline V₂O₅, and the small shift of band positions may relate to surface interaction between vanadium oxide and MCM-41. The V=O stretching frequency of the silica-supported vanadium species was reported to be closely associated with the degree of aggregation of vanadate into clumps.^{1–4,27} The supported vanadium oxide existed as isolated species, two-dimensional vanadate clusters (thin films), and bulk V₂O₅ crystallites give the V=O stretching mode at Raman bands of 1042, 1039, and 997 cm⁻¹, respectively.²⁷ Accordingly, the two-dimensional vanadate clusters were recommended to be the dominant vanadium species anchored on the surface of MCM-41 structure after calcination.

The Raman spectra of calcined VAPO-5 samples were shown in Figure 7. Except for a band at ~1022 cm⁻¹ (corresponding to V=O stretching of isolated vanadyl species), Raman features of calcined (in dry O₂) VAPO-5 sample at ~249 cm⁻¹ (ring breathing and distortion modes of T–O, T = Al or P), 403, 500 cm⁻¹ (T–O–T bending) and 1135 cm⁻¹ (T–O stretching) are similar to those of AlPO-5.²⁸ While VAPO-5 was calcined in air with some humidity, this led to the extraction of most of V atoms out of framework and the generation of extraframework vanadium species that results in a Raman spectrum characteristic of crystalline V₂O₅ (283, 403, 519, 700, and 993 cm⁻¹) as shown in Figure 6b.

In addition, Raman spectroscopy has also been shown to be an ideal technique for the study of conformational states of the hydrocarbon chains of cationic surfactant in the micelles,^{29,30} and micelles have been considered to be the template for synthesis of MCM-41. At room temperature, CTAB forms spherical micelles in an aqueous solution at concentrations between the cmc (critical micelle concentration, about 0.1 wt %) and ~10 wt %, while the transformation of spherical micelle to rod-shaped micelle and to hexagonal liquid-crystal phase transitions occur at about 10 and 28 wt % of surfactant concentration, respectively.^{19b} Raman spectra of synthetic Si-MCM-41 (Si-F) and V-MCM-41 (SiV30) samples are compared with those of CTAB molecules in solid and aqueous (20 wt % in water) forms as shown in Figure 8. Raman frequencies and their corresponding assignments²⁹ are summarized in Table 2.

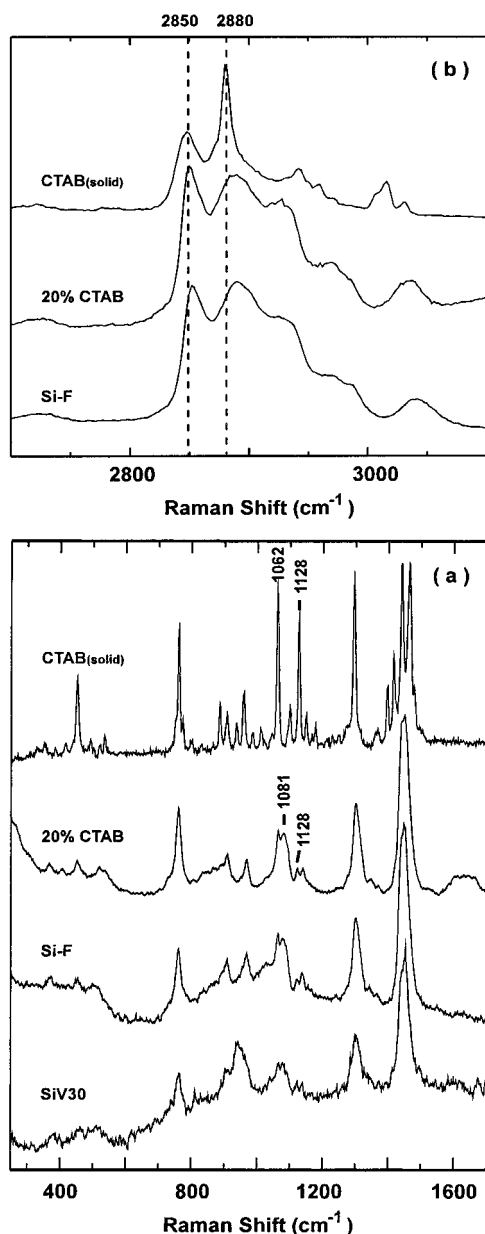


Figure 8. Raman spectra of CTAB in solid, aqueous solution (20% relative to water), as-synthesized Si-F and SiV30 in the range of (a) 250–1700 cm^{-1} and (b) 2700–3100 cm^{-1} .

The vibrational modes of CTAB encapsulated in either Si-F (synthesized from the reaction mixture containing $\sim 1\%$ CTAB) or SiV30 materials are similar to those observed in a nonsolid, micellar form of CTAB (20% CTAB in water) as shown in Figure 8. The intense Raman bands of 1062 and 1128 cm^{-1} of solid CTAB are corresponding to the symmetric and asymmetric C–C stretchings, respectively. These two bands are characteristic vibrations of an extended hydrocarbon chain with all-trans (ordered) structures in which the alternate carbon atoms move in the opposite direction. The longitudinal accordion mode and C–N stretching of CTAB give rise to the Raman features around 452 and 909 cm^{-1} , respectively. The vibrational modes of long-chain methylene exist at 959 cm^{-1} (rocking), 1293 cm^{-1} (twisting), and 1417, 1441 cm^{-1} (bending). The terminal methyl group of extended hydrocarbon chain exhibits the Raman band at 883 cm^{-1} (rocking), while the methyl groups from the polar head, $\text{N}(\text{CH}_3)_3^+$, give the Raman peaks around 759 cm^{-1} (rocking), 1368 cm^{-1} (C–CH₃ symmetric bending), and 1398 cm^{-1} (C–H symmetric bending). In addition, the weak bands at 1045 cm^{-1} (due to CH₂ twisting), 1100 cm^{-1}

TABLE 2: Raman Band Assignments of CTAB in Various Environments

Raman bands (cm^{-1}) of CTAB				assignment
solid	Si-F	SiV30	20% in H ₂ O	
452	452	464	460	longitudinal accordion mode
489				longitudinal accordion mode
537				longitudinal accordion mode
759	759	764	762	CH ₃ rock from $\text{N}(\text{CH}_3)_3$ group
774				CH ₃ rock from $\text{N}(\text{CH}_3)_3$ group
883	890		892	CH ₃ rock
909	910	910	912	C–N ⁺ stretch
937				
959	966	953	970	CH ₂ rock
987				CH ₂ rock
1011				
1045			1036	CH ₂ twist, crystalline
1062	1064	1066	1064	C–C sym str, + CH ₂ wag
	1079	1080	1084	gauche
1100				C–H str, crystalline
1128	1128	1125	1126	C–C asym str + CH ₂ wag
	1139	1136	1142	
1151				
1167				
1171				CH ₂ wag, crystalline
1212				CH ₂ wag, crystalline
1228				CH ₂ wag, crystalline
1249				CH ₂ wag, crystalline
1272				CH ₂ wag, crystalline
1293	1300	1302	1302	CH ₂ twist
1368				C–CH ₃ sym bending
1398				C–H sym bend from $\text{N}(\text{CH}_3)_3$
1417				–CH ₂ bend
1441	1446	1454	1440	–CH ₂ bend
1465	1462		1456	–CH ₂ bend, crystalline
1480				

(due to C–C stretching), and 1171 cm^{-1} (due to CH₂ wagging), and the intense band at 1465 cm^{-1} (due to CH₂ bending) belong to the vibrations of CTAB in the all-trans crystalline state. The ~ 2850 (~ 2930) and ~ 2890 (~ 2960) cm^{-1} peaks correspond to the C–H symmetric and asymmetric stretching of CH₂ (CH₃), respectively.³⁰

In comparison with solid CTAB that exists in all-trans structures of a crystalline state, the occluded CTAB in MCM-41 exhibits the features of liquidlike structures. The band at about 1079 cm^{-1} (occurring in encapsulated CTAB of MCM-41) or at 1081 cm^{-1} (appearing in aqueous form, 20% in water) has not been observed in the solid surfactant and is ascribed to C–C stretching mode of hydrocarbon chains with several gauche (disordered) configurations. The CTAB molecules in a spherical micellar core or in a rod-shaped structure would generate this kind of bands.²⁹ The Raman bands of a crystalline CTAB at about 1045, 1171, and 1465 cm^{-1} were absent in the occluded or liquid-formed CTAB. These differences imply that hydrocarbon chains of CTAB in the mesopores of MCM-41 behave like in a fluid state and exhibit various structures which include several gauche rotations. The relative peak-intensity ratios of I_{1081}/I_{1128} and I_{2850}/I_{2890} can be used as a disorder/order (or gauche/trans) parameter to estimate the degree of disorder of an extended hydrocarbon chains by Raman spectroscopy.^{29,30} The occluded CTAB in mesoporous MCM-41 gives higher ratios of I_{1079}/I_{1128} and I_{2850}/I_{2890} than CTAB in the form of rodlike aggregate (20% CTAB in water), indicating a higher rigidity of hydrocarbon chains in the CTAB micelle of MCM-41. The interaction between CTAB and silicate is expected to induce some rigidity to the rodlike micelle, although the surfactant has only been introduced at very low concentration in the reaction mixture (1% CTAB). The templating effect of CTAB molecules in the formation of mesoporous MCM-41 molecular sieve can therefore be monitored by Raman spec-

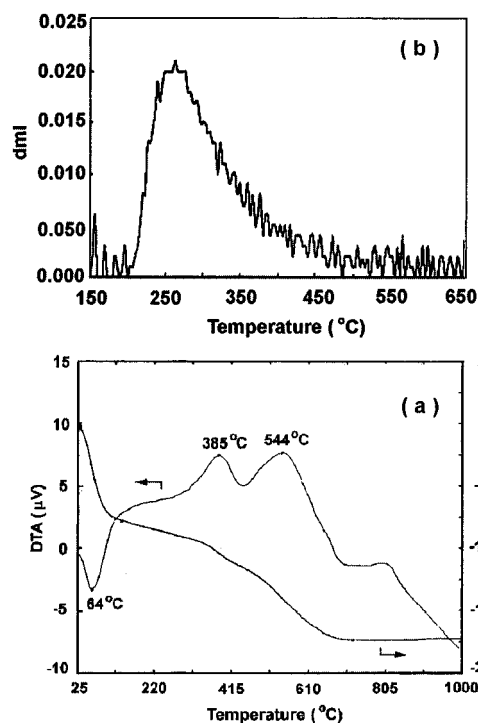


Figure 9. (a) TG/DTA profile of as-synthesized VAPO-5 and (b) TPD of NH₃ profile of NH₃ adsorbed, calcined VAPO-5.

troscopy. Furthermore, Raman band of CH₃ rocking of -N(CH₃)₃ (polar-end group) occurs at a slightly different position 759 cm⁻¹ for synthetic Si-F and 764 cm⁻¹ for SiV30. An interaction between the hydrophilic end group of CTAB, -N(CH₃)₃, and silanol groups in Si-F or V-OH in SiV30 may induce such variance.

TG/DTA analysis. Figure 9a shows the TG and DTA spectra of synthetic VAPO-5 sample. The low-temperature (30–150 °C) endotherm with weight loss of 7.77% is associated with the desorption of water. The exothermic peaks at 315–435 and 435–700 °C may be the result of the decompositions of neutral Pr₃N molecules and protonated Pr₃NH⁺ cations, respectively. As suggested by Rigutto *et al.*,¹⁵ during the crystallization of VAPO-5, nontetrahedral VO²⁺ ions may replace tetrahedral Al³⁺ ions and this leads to an anionic framework counterbalanced by Pr₃NH⁺ cations; this is similar to Et₃NH⁺ ions in CoAPO-5 or SAPO-5.³⁴

TPD of Ammonia. The profile of TPD of ammonia for calcined and NH₃-adsorbed VAPO-5 sample is shown in Figure 9b. The peak at around ~267 °C may be assigned to structural acidity derived from medium-strong acidic V-OH groups in VAPO-5 molecular sieve. The acid strength was found to be lower than that observed in CoAPO-5 and SAPO-5.³¹

HREM and EDS Spectroscopy. EDS spectroscopy can be used to analyze a particular element quantitatively in a matrix over the area of interest under electron microscopy. The combination of high-resolution transmission electron microscopy (HRTEM) and EDS with nanosize probe is capable of retrieving the information about the microstructure and the corresponding composition of a sample at the nanometer scale.³²

An EDS spectrum of calcined SiV30 sample (Si/V ≈ 51 by ICP), with the probing size of about 50 Å in diameter, is shown in Figure 10c. Table 3 records in the analytical results of elemental compositions over various positions of calcined SiV30 particles and it shows the local distributions of vanadium ions at nanometer resolution. It should be noteworthy that the intensity of vanadium signal seems to vary with the orientation of hexagonal channels of V-MCM-41. When the direction of

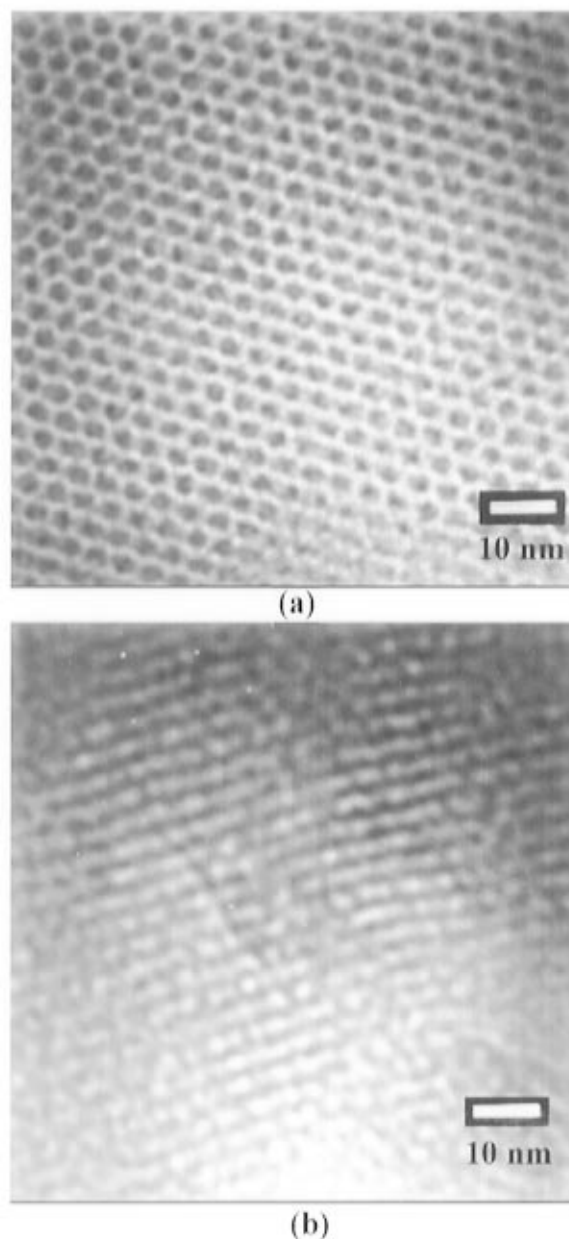
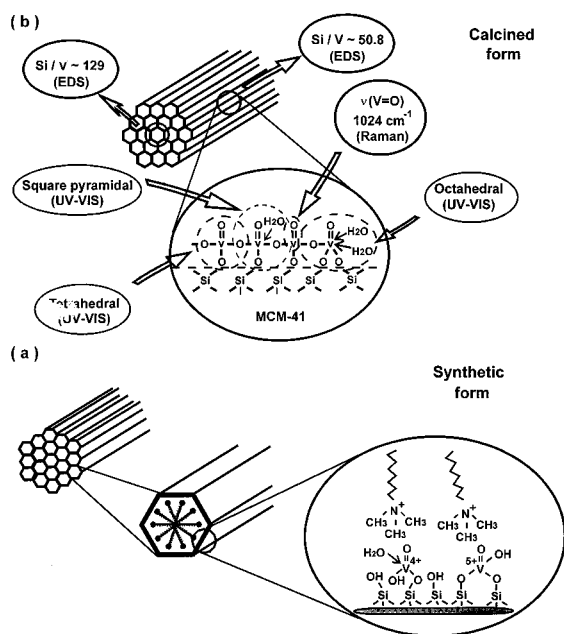


Figure 10. (c) EDS spectrum and (a, b) HREM micrographs of calcined SiV30 sample in different orientations.

TABLE 3: Chemical Composition of the Calcined V-MCM-41 (SiV30) Material Analyzed by EDS

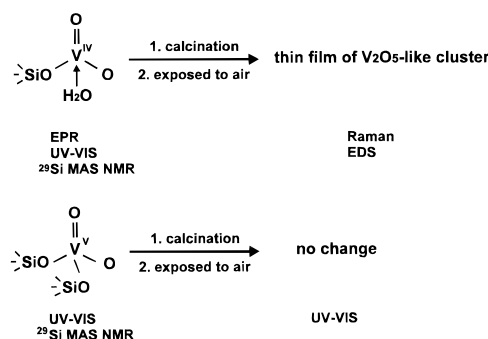
run	atomic concentration (%)		Si K α /V K α
	Si K α	V K α	
(a) Tubular Wall			
1	97.1	2.95	
2	99.2	0.85	
3	99.0	0.98	
4	98.1	1.94	
5	100	0.00	
6	97.7	2.34	
7	97.2	2.83	
8	98.6	1.37	
9	95.6	4.42	
10	98.4	1.64	
av	98.1 \pm 1.26	1.93 \pm 1.26	50.8 \pm 1.00
(b) Hexagonal Array			
1	99.5	0.52	
2	99.3	0.66	
3	97.9	2.06	
4	98.5	1.53	
5	99.2	0.76	
6	98.8	1.16	
7	99.3	0.73	
8	100	0.00	
9	99.7	0.26	
10	100	0.00	
av	99.2 \pm 0.626	0.77 \pm 0.626	129 \pm 1.00

SCHEME 1: Proposed Scheme of Vanadium Interacting with MCM-41 Structure (a) before and (b) after Calcination

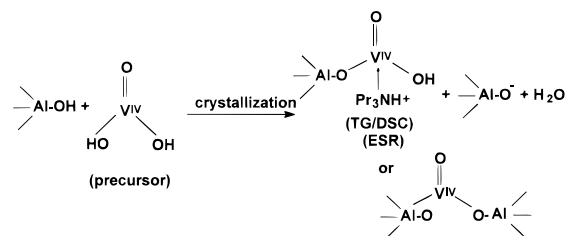
electron beam irradiated the sample was parallel to the hexagonal arrays of V-MCM-41, as shown by the image in Figure 10a, the higher atomic ratio 129 of Si/V (from Si and V K α edges) was found, and this is consistent with the ESCA analysis that gives a ratio of ~ 121 .³³ On the other hand, the smaller Si/V atomic ratio of 50.8 was observed by directing electron beam perpendicular to the hexagonal arrays (the image shown in Figure 10b), in an agreement with the bulk result of ~ 52 by ICP-AES. The above results reveal that the vanadium distribution is not uniform through channels of MCM-41 framework and the enrichment of vanadium species on the channel walls was found.

Discussion

According to the investigations by EPR and UV-vis, synthetic V-MCM-41 samples possess two types of vanadium species, the monodispersed ions ($V^{IV}=O$)²⁺ in a tetrahedral coordination, and the tetrahedral ($V^V=O$)³⁺ ions in the lattice of MCM-41. It is likely that these vanadyl ions are grafted on the surface of the tubular walls of MCM-41 by condensation with silanol groups of walls. Such grafting, in turn, induces a decrease of silanol species as detected by ²⁹Si MAS NMR, and the end product is present as surface-bound vanadyl species in the form of ($\equiv SiO$) $V^{IV}O(OH)$ or ($\equiv SiO$)₂ $V^VO(OH)$, as in the case of V-silicalite.² Such coordination through grafting is not very rigid and this suggests that some mobility of the vanadium atom exists, especially in the case of single-bonded Si-O-V connection. Upon calcination, the isolated ($V^{IV}=O$)²⁺ ions of ($\equiv SiO$) $V^{IV}O(OH)$ were completely oxidized to ($V^V=O$)³⁺ ions and, after exposure to air, they further aggregated into two-dimensional vanadate chains, and these aggregates are nonuniformly distributed on the tubular walls of hexagonal arrays of MCM-41 as demonstrated by Raman spectroscopy and by the combination of EDS and HRTEM measurements. The oligomerization of the vanadium species upon hydration was also observed in the case of V-MCM-48,⁷ while the tetrahedral ($V^V=O$)³⁺ ions of ($\equiv SiO$)₂ $V^VO(OH)$ (incorporated in the lattice) may still remain stable in the framework of MCM-41 after calcination. Based on the above discussions, the plausible structures of the different V species in as-synthesized and calcined V-MCM-41 samples are suggested as follows:



On the other hand, two types of vanadyl ($V^{IV}=O$)²⁺ ions with slightly different environment were found in as-synthesized VAPO-5 by EPR investigation. Similar to V-MCM-41, these vanadyl ions may be localized on the inner surface of the one-dimensional channel system via a condensation with hydroxyl groups of Al-OH, as proposed in the following:



During calcination, ($V^{IV}=O$)²⁺ is very sensitive to the presence of water vapor and is partially oxidized to either isolated square pyramidal ($V^V=O$)³⁺ species (in dry O₂) or V₂O₅ cluster (in air with humidity), as identified by Raman. Following the H₂ treatment at 500 °C, the calcined VAPO-5 sample with the isolated ($V^V=O$)³⁺ species possesses the higher reactivity toward O₂ than VAPO-5 sample with aggregated V₂O₅, as based on EPR results.

Conclusions

Vanadium can be incorporated in the tubular wall of MCM-41 through interaction with surface silanol groups; in VAPO-5, the vanadyl ions are stabilized on the internal surface of pore system via condensation with hydroxyl groups of Al-OH. Upon calcination and exposure to air, a thin film of vanadate is nonuniformly deposited on the wall-surface of MCM-41 support, while the ease of vanadium (V^{4+}) oxidation in as-synthesized VAPO-5 sample is mainly dependent on the calcination condition. The presence of water vapor will facilitate the oxidation of $(V^{IV}=O)^{2+}$ and form V_2O_5 cluster instead of isolated $(V^V=O)^{3+}$ species. The location and migration of these vanadium species in MCM-41 are shown in Scheme 1.

Acknowledgment. The authors are grateful to Professor Fu-Rong Chen for the discussion and access to HRTEM and EDS. This work was supported in part by the National Science Council of Republic of China.

References and Notes

- (1) Das, N.; Eckert, H.; Hu, H.; Wachs, I. E.; Walzer, J. F.; Feher, F. *J. Phys. Chem.* **1993**, *97*, 8240.
- (2) Whittington, B. I.; Anderson, J. R. *J. Phys. Chem.* **1993**, *97*, 1032.
- (3) (a) Oyama, S. T.; Went, G. T.; Lewis, K. B.; Bell, A. T.; Somorjai, G. A. *J. Phys. Chem.* **1989**, *93*, 6786. (b) Went, G. T.; Oyama, S. T.; Bell, A. T. *J. Phys. Chem.* **1990**, *94*, 4240.
- (4) Roozeboom, F.; Mittelmeijer-Hazeleger, M. C.; Moulijn, J. A.; Medema, J.; de Beer, V. H. J.; Gellings, P. J. *J. Phys. Chem.* **1980**, *84*, 2783.
- (5) (a) Reddy, K. M.; Moudrakovski, I.; Sayari, A. *J. Chem. Soc., Chem. Commun.* **1994**, 1059. (b) Reddy, J. S.; Sayari, A. *J. Chem. Soc., Chem. Commun.* **1995**, 2231.
- (6) Gontier, S.; Tuel, A. *Microporous Mater.* **1995**, *5*, 161.
- (7) Morey, M.; Davidson, A.; Eckert, H.; Stucky, G. *Chem. Mater.* **1996**, *8*, 486.
- (8) Moudrakovski, I.; Sayari, A.; Ratcliffe, C. I.; Ripmeester, J. A.; Preston, K. F. *J. Phys. Chem.* **1994**, *98*, 10895.
- (9) (a) Kornatowski, J.; Sychev, M.; Kuzenkov, S.; Strnadova, K.; Pilz, W.; Kassner, D.; Pieper, G.; Bauer, W. H. *J. Chem. Soc., Faraday Trans.* **1995**, *91*, 2217. (b) Kornatowski, J.; Wichterlova, B.; Jirkovsky, J.; Löffler, E.; Pilz, W. *J. Chem. Soc., Faraday Trans.* **1996**, *92*, 1067.
- (10) Centi, G.; Perathoner, S.; Trifiro, F.; Aboukais, A.; Aissi, C. F.; Guelton, M. *J. Phys. Chem.* **1992**, *96*, 2617.
- (11) Bellussi, G.; Maddinelli, G.; Carati, A.; Gervasini, A.; Millini, R. In *Proceedings of the 9th International Zeolite Conference* van Ballmoos, R., Higgins, J. B., Treacy, M. M. J., Eds.; Butterworth-Heinemann: Stoneham, 1993; p 207.
- (12) Sen, T.; Ramaswamy, V.; Ganapathy, S.; Rajamohanan, P. R.; Sivasanker, S. *J. Phys. Chem.* **1996**, *100*, 3809.
- (13) Montes, C.; Davis, M. E.; Murray, B.; Narayana, M. *J. Phys. Chem.* **1990**, *94*, 6431.
- (14) Jhung, S. H.; Uh, Y. S.; Chon, H. *Appl. Catal.* **1990**, *62*, 61.
- (15) Rigutto, M. S.; van Bekkum, H. *J. Mol. Catal.* **1993**, *81*, 77.
- (16) Weckhuysen, B. M.; Vannijvel, I. P.; Schoonheydt, R. A. *Zeolites* **1995**, *15*, 482.
- (17) Lohse, U.; Brückner, A.; Kintscher, K.; Parltz, B. *J. Chem. Soc., Faraday Trans.* **1995**, *91*, 1173.
- (18) (a) Beck, J. S.; Vartuli, J. C.; Roth, W. J.; Leonowicz, M. E.; Kresge, C. T.; Schmitt, K. D.; Chu, C. T.; Olsen, D. H.; Sheppard, E. W.; McCullen, S. B.; Higgins, J. B.; Schlenker, J. L. *J. Am. Chem. Soc.* **1992**, *114*, 10834. (b) Kresge, C. T.; Leonowicz, M. E.; Roth, W. J.; Vartuli, J. C.; Beck, J. S. *Nature* **1992**, *359*, 710.
- (19) (a) Monnier, A.; Schuth, F.; Huo, Q.; Kumar, D.; Margolese, D.; Maxwell, R. S.; Stucky, G. D.; Krishnamurty, M.; Pertoff, P.; Firouzi, A.; Janicke, M.; Chmelka, B. F. *Science* **1993**, *261*, 1299. (b) Huo, Q.; Margolese, D.; Ciesla, U.; Demuth, D. G.; Feng, P.; Gier, T. E.; Sieger, P.; Firouzi, A.; Chmelka, B. F.; Schuth, F.; Stucky, G. D. *Chem. Mater.* **1994**, *6*, 1176. (c) Firouzi, A.; Kumar, D.; Bull, L. M.; Besier, T.; Sieger, P.; Huo, Q.; Walker, S. A.; Zasadzinski, J. A.; Glinka, C.; Nicol, J.; Margolese, D.; Stucky, G. D.; Chmelka, B. F. *Science* **1995**, *267*, 1138.
- (20) Chen, C. Y.; Li, H.-X.; Davis, M. E. *Microporous Mater.* **1993**, *2*, 17.
- (21) Wu, C. N.; Tsai, T. S.; Liao, C. N.; Chao, K. J. *Microporous Mater.* **1996**, *7*, 173.
- (22) Shvets, V. A.; Kazansky, V. B. *J. Catal.* **1972**, *25*, 123.
- (23) Che, M.; Tench, A. J. *Adv. Catal.* **1982**, *31*, 77.
- (24) Selig, H.; Claassen, H. H. *J. Chem. Phys.* **1966**, *44*, 1404.
- (25) Miller, F. A.; Cousins, L. R. *J. Chem. Phys.* **1957**, *26*, 329.
- (26) Miller, F. A.; Baer, W. K. *Spectrochim Acta* **1961**, *17*, 112.
- (27) Okuhara, T.; Inumaru, K.; Misono, M.; Matsubayashi, N. In *New Frontiers in Catalysis: Proceedings of the 10th International Congress on Catalysis*; Gucci et al., Eds.; Elsevier: New York, 1993; p 1767.
- (28) Holmes, A. J.; Kirkby, S. J.; Ozin, G. A. Young, D. *J. Phys. Chem.* **1994**, *98*, 4677.
- (29) Kalyanasundaram, K.; Thomas, J. K. *J. Phys. Chem.* **1976**, *80*, 1462.
- (30) Amorim da Costa, A. M.; Geraldine, C. F. G. C.; Teixeira-Dias, J. J. C. *J. Colloid Interface Sci.* **1992**, *86*, 254.
- (31) Chao, K. J.; Sheu, S. P.; Chen, S. H.; Lin, J. C.; Lievens, J. In *Synthesis of Microporous Materials*; Occelli, M. L., Robson, H. E., Eds.; Van Nostrand Reinhold: New York, 1992; Vol. 1, p 317.
- (32) Stadelmann, P.; Leifer, K.; Verdon, C. *Ultramicroscopy* **1995**, *58*, 35.
- (33) Lin, L. H. Ph.D. Thesis, National Tsinghua University, 1995.